Pb m –Phenyl (m = 1–5) Complexes: an Anion Photoelectron Spectroscopy and Density Functional Study

ARTICLE *in* THE JOURNAL OF PHYSICAL CHEMISTRY A · AUGUST 2006

Impact Factor: 2.69 · DOI: 10.1021/jp0617470 · Source: PubMed

5 AUTHORS, INCLUDING:

Xiaopeng Xing
Tongji University
36 PUBLICATIONS **492** CITATIONS
SEE PROFILE

Zhen Gao
Chinese Academy of Sciences
39 PUBLICATIONS **347** CITATIONS
SEE PROFILE

Zichao Tang
Chinese Academy of Sciences
66 PUBLICATIONS **514** CITATIONS
SEE PROFILE

Phenyl-Coinage Metal (Ag, Au) Complexes: an Anion Photoelectron Spectroscopy and Density Functional Study

Shutao Sun, Xiaopeng Xing, Hongtao Liu, and Zichao Tang*

State Key Laboratory of Molecular Reaction Dynamics, Center of Molecular Science, Institute of Chemistry, Chinese Academy of Sciences, Beijing 100080, P. R. China

Received: July 22, 2005; In Final Form: October 20, 2005

The important intermediate phenyl-coinage metal complexes ($Ag_mC_6H_5^-$, $Au_mC_6H_5^-$), which are produced from the reactions between coinage metal clusters formed by laser ablation and the benzene molecules seeded in argon carrier gas, are studied by PES (photoelectron spectroscopy) and DFT (density functional theory). The EAs (adiabatic electron affinities) of these complexes are obtained from PES at both 308 and 193 nm photon energies and show odd−even alternation. Calculations with DFT are carried out on the structural and electronic properties of $Ag_mC_6H_5^-$ and $Au_mC_6H_5^-$; the adiabatic detachment energy and the calculated DOS (density of states) for the ground state of a given anion are in good agreement with the experimental PES results. The observed spectra are also compared with those of the pure coinage metal clusters, which reveal that there are some similarities between them and the phenyl acts like an additional metal atom in the clusters. Furthermore, the bonding between phenyl and metal is analyzed, suggesting that phenyl group binds perpendicularly on metal clusters through C−M σ bond.

1. Introduction

In recent years, there has been considerable interest in the properties of nanosized coinage (Ag, Au) clusters serving as building blocks of nanostructured materials[1−4] and novel nanocatalytic systems.[5−9] And gas-phase coinage (Ag, Au) clusters are suitable model systems to shed light on reaction mechanisms of Ag-based and Au-based catalysis.[10−12] Ag_m and Au_m (m = 1−3) are the smallest coinage nanosized catalytic clusters, they are the basic constituent for the larger nanomaterials and nanocatalytic systems.

Moreover, adsorption of molecules or fragments on coinage metal (Ag, Au) surfaces is an important field in surface science.[13−16] Verifying the structures and properties of the adsorbates on these metals can develop a microscopic level description of many heterogeneous catalytic reactions (for example, the Ullmann reactions[17]). Because the active points in the catalytic reactions are localized near the edges or the defects of metal surfaces, studying on the fragments adsorbed on small metal clusters can be a promising platform for catalysis and nanoassembly. It is just as the recognition that the cluster science not only can elucidate the properties of condensed phase but also can provide detailed information on the reaction mechanisms and the nature of the reaction sites that enable certain catalytic substance to be especially effective.

Benzene is one of the most important organic molecules in chemistry and biology. The interaction of coinage metal clusters with benzene molecules will be fundamental to nanoscale catalysis and materials. Phenyl groups adsorbed on bulky silver and gold surfaces has been well characterized using HREEL,[14] NEXAFS[15] and IRAS[16] methods, which indicates that the phenyl group on orderly coinage metal surfaces has a slightly tilted configuration through the metal−carbon bond. And there are a lot of experimental[18−25] and theoretical[26−28] investigations on the interaction of metal clusters with benzene. However, the species of phenyl coupled on the metal atom or clusters are very rare cases in chemistry.

Here we report the first observation of the intermediate phenyl-coinage metal complexes $M_mC_6H_5^-$ (M = Ag, Au; m = 1−3) in the gas phase from reactions between benzene and coinage metals by laser vaporization. The products are measured by a reflectron time-of-flight mass spectrometer and anion photoelectron spectroscopy. Photoelectron spectroscopy is a well-known powerful experiment technique to provide direct molecular electronic structure information and there are lots of studies on structures of coinage metal clusters using PES.[29−33] In this work, the bonding, geometric and electronic structures of these complexes $M_mC_6H_5^-$ (M = Ag, Au; m = 1−3) are obtained by a combination of experimental and theoretical studies. The results in this study will provide the fundamental information for future studies of the physics and chemistry for these systems.

2. Experimental Methods

The pure metal disk targets are ablated by a pulsed laser beam (532 nm Nd:YAG laser, 10 mJ/pulse) and the targets are rotated during the experiment. The laser-induced plasma is mixed with benzene (analytical reagent) in a channel and the benzene is seeded in argon (purity 99.99%) carrier gas delivered by a pulsed valve at a backing pressure of about 400 kPa. The volume ratio of benzene in the mixed gas is about 0.2%. The phenyl-coinage metal clusters formed are entrained with the carrier gas and undergo a supersonic expansion. After passing a skimmer, all products are into the accelerating area, and then negatively charged clusters are extracted perpendicularly from the collimated cluster beam for size analysis by a reflectron time-of-flight mass spectrometer. The resolution ($M/\Delta M$) of the mass spectrometer is about 2000, so it is easy to resolve the number of the hydrogen atoms in the products. The products of interest are mass selected and photodetached by a XeCl excimer laser

* Corresponding author. E-mail: zctang@iccas.ac.cn.

10.1021/jp054068i CCC: $30.25
Published on Web 12/06/2005

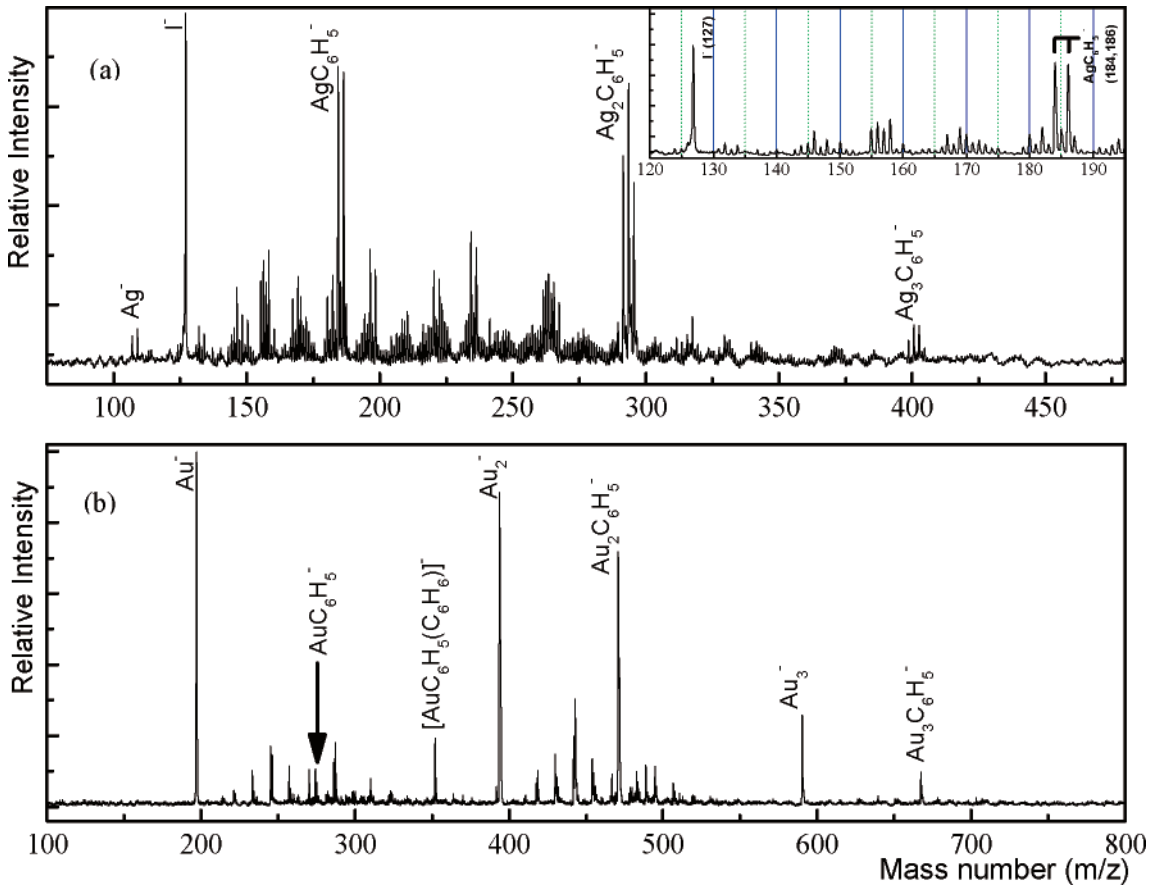

Figure 1. Typical mass spectra of the anionic products by laser ablation of coinage metal samples (a, Ag; b, Au) into a mixture of benzene and argon (0.2% benzene in 400 kPa mixed gas). The inset in (a) shows the enlarged part of the spectra, which contain $AgC_6H_5^-$ and I^- mass peaks.

(308 nm) and an ArF excimer laser (193 nm), respectively. Photoelectrons are measured by a magnetic-bottle time-of-flight analyzer and calibrated by the known spectra of Ag^- and Au^-. The energy resolution of the instrument is approximately 70 meV for 1 eV electrons. Details of the apparatus have been published elsewhere.[34,35]

3. Computational Methods

Full geometric optimization for all the cluster structures is performed with relativistic density functional calculations at the level of generalized gradient approach using a Perdew−Wang exchange-correlation functional.[36] The zero-order regular approximation Hamiltonian is used to account for the scalar (mass velocity and Darwin) relativistic effects.[37] The standard Slater-type orbital basis sets of the triple-ζ plus two polarization functions (TZ2P) are used for the orbitals of Au, Ag, C, and H atoms. And the frozen core ($1s^2-3d^{10}$) approximation, ($1s^2-4f^{14}$) approximation is used for Ag and Au, respectively. The DOS spectra are obtained by Lorentzian extensions of the discrete single particle energy levels with a width $\sigma = 0.1$ eV. All the calculations are accomplished with the Amsterdam Density Functional (ADF 2002) programs.[38] It has been shown previously that these theoretical methods are suitable for studying the coinage metal clusters.[39]

4. Results and Discussion

4.1. Mass Spectra. As shown in Figure 1, $M_mC_6H_5^-$ (M = Ag, Au; $m = 1-3$) are the dominant products of the reactions. The I^- peak present (coming from the trace CH_3I mixed in argon purposively) is very helpful for assignment of the products. The formation mechanism is proposed as

$$M_m^- + C_6H_6 \rightarrow [M_m\cdots(C_6H_6)]^{-*} \xrightarrow{Ar} M_mC_6H_5^- + H \quad (1)$$

The mechanism of these complexes has been discussed in detail in our former publication,[22] and it surely involves the selective C−H cleavage of benzene due to the negative charge and the excessive energy in the metal clusters. The product $M_mC_6H_5^-$ can adsorb another benzene molecule to form $[M_mC_6H_5(C_6H_6)]^-$ species or adsorb other fragments, and this is the reason $M_mC_6H_5^-$ is seen as an intermediate complex.

4.2. 193 nm Spectra. The photoelectron spectra represent transitions from the ground state of the anions to the ground and excited electronic states of the neutrals. The anions are in their electronic ground state because they are cooled in a supersonic expansion. When the photodetachment process happens, this process is much faster compared with the movements of the nuclei. Consequently, PES provides the electronic and vibrational (if the resolution is enough) information of the neutral species corresponding to the anionic cluster geometry. EA is defined as the energy of the origin transition between the ground state of the anion and the ground state of the neutral.

The most obvious characteristic in the spectra is that the phenyl-coinage metal complexes, both Ag and Au, show the odd−even alternation of EAs. The species containing odd numbers of metal atoms, AgC_6H_5, $Ag_3C_6H_5$, AuC_6H_5 and $Au_3C_6H_5$, exhibit lower electron binding energies and large energy gaps, which indicates that the neutral clusters are closed-shell, and their highest-occupied-molecular orbital (HOMO) is

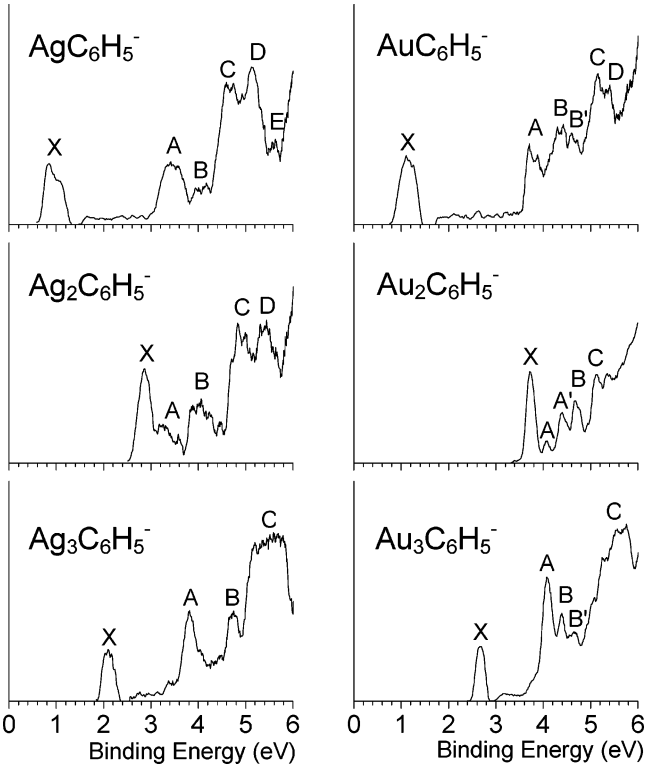

Figure 2. Photoelectron spectra of $M_mC_6H_5^-$ (M = Ag and Au; m = 1−3) at 193 nm (6.42 eV) photon.

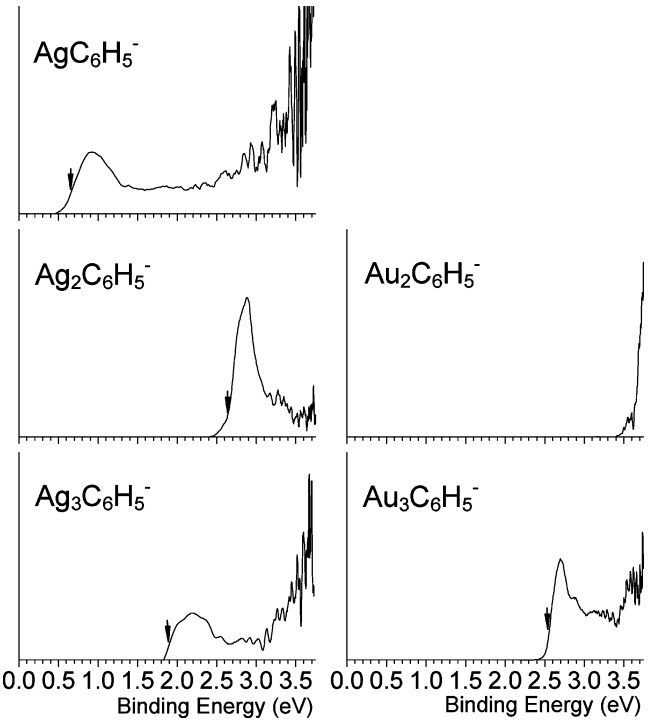

Figure 3. Photoelectron spectra of $M_mC_6H_5^-$ (M = Ag and Au; m = 1−3) at 308 nm (4.03 eV) photon.

occupied by two electrons, the charging electron, which makes the species negative, would occupy the lowest-unoccupied-molecular orbital (LUMO). The HOMO−LUMO energy gap of AgC_6H_5 is larger than $Ag_3C_6H_5$, and AuC_6H_5 is larger than $Au_3C_6H_5$. However, the clusters containing even numbers of metal atoms, $Ag_2C_6H_5$ and $Au_2C_6H_5$, show higher electron binding energy, which suggests that they are open-shell electronic systems. Their HOMO is occupied by only one

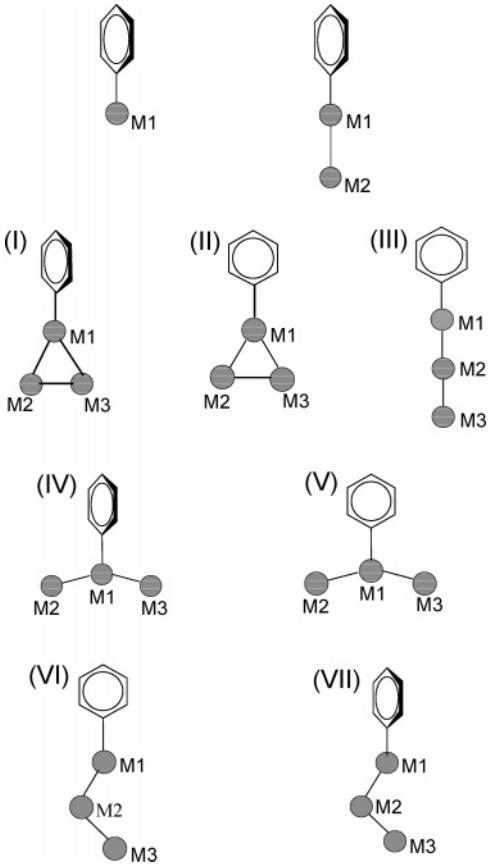

Figure 4. Optimized structures for neutral and anionic complexes of $M_mC_6H_5$ (M = Ag and Au; m = 1−3). See Table 1 for structural parameters.

electron, so the charging electron would occupy the other position of the HOMO, which makes their EAs higher. This can be explained by the electron pairing effect, just like the pure coinage metal clusters, in which the EA of the odd-numbered pure metal cluster is larger than that of an even one.[29−32] Because each metal atom in the clusters contributes a single s valence electron to the bonding orbitals, the odd-numbered pure coinage metal anionic clusters are closed-shell. The electron in a doubly occupied HOMO will feel a stronger effective core potential due to less effect of the electron screening for electrons in the same orbital than for the inner shell electrons. By this analysis, the C_6H_5 group acts like an additional coinage metal atom in these complexes that it contributes a single electron to bond with the metal fragment. From this point, the PES of M_m^- and $M_{m-1}C_6H_5^-$ should have some similarities if their geometry structures are similar. We will discuss it later. We also note that EAs of $Au_mC_6H_5$ are larger than $Ag_mC_6H_5$, especially remarkable for $M_2C_6H_5^-$. This is derived from the contraction effect of the 6s orbital and the stability effect of the relativistic effect of Au, which enhanced the binding effect of the charging electron to the clusters, especially stabilized for the closed-shell anionic complex.

For MC_6H_5 and $M_3C_6H_5$ neutral complexes, their HOMOs are doubly occupied, the first feature X in the spectra corresponds to their ground state, and the second feature A corresponds to the first excited state, in which an electron in the HOMO is transited to the LUMO. Therefore, the energy difference between the first two features corresponds to the HOMO−LUMO gap. Whereas, the HOMO of $M_2C_6H_5$ is singly occupied, so there are two possibilities as to the first excited state, one is electron excitation from the HOMO to the LUMO

TABLE 1: Various Structural and Energetic Characteristics for Neutral and Anionic Complexes of $M_mC_6H_5$ (M = Ag and Au; $m = 1-3$)

									EA (eV)	
	isomer	state	point group	R_{C-M1} (Å)	R_{M1-M2} (Å)	R_{M2-M3} (Å)	$\theta_{M1-M2-M3}$ (deg)	ΔE^a (eV)	cal	exp[b]
AgC_6H_5		$^1A_1$	C_{2v}	2.08				0.00	0.75	0.66
$AgC_6H_5^-$		$^2A_1$	C_{2v}	2.18				0.00		
$Ag_2C_6H_5$		$^2A_1$	C_{2v}	2.11	2.62			0.00	2.60	2.66
$Ag_2C_6H_5^-$		$^1A_1$	C_{2v}	2.13	2.63			0.00		
$Ag_3C_6H_5$	I	$^1A_1$	C_{2v}	2.08	2.73	2.73	61.4	0.00	1.82	1.88
	II	$^1A_1$	C_{2v}	2.09	2.73	2.73	61.4	0.03	1.84	
	III		C_{2v}	2.08	2.70	2.60	180.0	0.72	2.39	
	VI		C_s	2.11	2.68	2.64	63.3	0.05	1.72	
	VII		C_1	2.09	2.67	2.63	63.4	0.03	1.70	
$Ag_3C_6H_5^-$	I	$^2B_2$	C_{2v}	2.12	2.73	2.73	60.2	0.00		
	II	$^2B_1$	C_{2v}	2.12	2.73	2.73	60.2	0.01		
	III		C_{2v}	2.13	2.70	2.62	180.0	0.15		
	VI		C_s	2.13	2.70	2.63	165.1	0.15		
	VII		C_1	2.13	2.70	2.63	165.1	0.15		
AuC_6H_5		$^1A_1$	C_{2v}	2.00				0.00	0.84	0.80
$AuC_6H_5^-$		$^2A_1$	C_{2v}	2.12				0.00		
$Au_2C_6H_5$		$^2A_1$	C_{2v}	2.02	2.59			0.00	3.32	3.52
$Au_2C_6H_5^-$		$^1A_1$	C_{2v}	2.03	2.61			0.00		
$Au_3C_6H_5$	I	$^1A_1$	C_{2v}	2.02	2.71	2.71	61.5	0.00	2.57	2.53
	II	$^1A_1$	C_{2v}	2.02	2.71	2.71	61.5	0.10	2.65	
	III		C_{2v}	2.00	2.67	2.57	180.0	0.74	3.22	
	IV		C_{2v}	2.02	2.57	2.57	5.5	0.73	2.56	
	V		C_{2v}	2.04	2.58	2.58	10.8	0.82	2.76	
	VI		C_s	2.01	2.59	2.53	126.8	0.14	2.64	
	VII		C_1	2.00	2.58	2.53	131.5	0.12	2.64	
$Au_3C_6H_5^-$	I	$^2B_2$	C_{2v}	2.03	2.74	2.74	61.0	0.00		
	II	$^2B_1$	C_{2v}	2.03	2.74	2.74	61.0	0.02		
	III		C_{2v}	2.04	2.66	2.61	180.0	0.10		
	IV		C_{2v}	2.04	2.64	2.64	16.3	0.76		
	V		C_{2v}	2.05	2.65	2.65	18.6	0.63		
	VI		C_s	2.04	2.66	2.61	164.7	0.08		
	VII		C_1	2.03	2.61	2.62	147.2	0.05		

[a] ΔE is the difference of complex energy relative to the correspondingly lowest lying structure. [b] The uncertainty for the experimental EA is ±0.05 eV.

and the other is from the HOMO−1 to the HOMO, and this can be assigned by the theoretical calculation. From the observed spectra, we can see that the HOMO−LUMO energy gap is larger for MC_6H_5 than for $M_3C_6H_5$ and the first excitation energy is the smallest one for the open-shell neutral complexes $M_2C_6H_5$.

4.3. 308 nm Spectra. Because no vibrational structures are observed, the position indicated by the arrow is evaluated to be the EA of the corresponding complexes in 308 nm spectra to take into account the instrumental resolution. In 193 nm spectra, the sharp onset of the first peak defines a fairly accurate EA of the corresponding complexes. The spectra at 308 nm photons are much better resolved for the low binding energy features accessible at this photon energy. In particular, the weak feature in the low binding energy area of $Au_2C_6H_5$ can be seen clearly, which cannot be recognized from the 193 nm spectra—there is a weak peak with a VDE (vertical detachment energy) of 3.55 eV before the strong peak with a VDE of 3.72 eV; we assign this weak feature due to little contamination.

4.4. Low Energy Structures. For both the neutral $M_mC_6H_5$ and anion $M_mC_6H_5^-$ (M = Ag and Au; $m = 1-3$), we consider many structures with different geometries. The optimized low-energy structures are shown in Figure 4 and their structural and energetic characteristics are summarized in Table 1. For neutrals and anions of $M_mC_6H_5$ (M = Ag and Au; $m = 1, 2$), their optimized structures are C_{2v} symmetry, in which the phenyl group couples on a metal atom through a C−M bond and the phenyl and metal atoms are coplanar. The other initial structures collapse to this geometry during optimization. For neutrals and anions of $M_3C_6H_5$ (M = Ag and Au), there are some low-energy isomeric structures (I−VII); the geometry of the lowest energy is a C_{2v} symmetry where the phenyl group is perpendicular to the plane of M_3 cluster. The energy of another C_{2v} structure in which the phenyl group rotates to the same plane of M_3 cluster is only slightly higher than the former one. For the neutral and anion of $Ag_3C_6H_5$, there are no optimized structures IV and V, for they collapse to structures I and II. The C−M bond lengths obtained here are similar to the results of another theoretical study based on MP2/I level (the differences are within 0.02 Å).[40] Additionally, in the same $M_m-C_6H_5$ series, the bond lengths always have the trend of Ag−C > Au−C, which is attributed to the relativistic effect.

4.5. Assignments of the Complex Structures. In the following, we confirm the C_{2v} structures of $M_mC_6H_5$ (M = Ag and Au; $m = 1-3$) by the calculated EAs using the relativistic DFT and assign the most possible structures for $M_3C_6H_5$ on the basis of relative energies and comparisons between the theoretically calculated DOS spectra and the experimental PES spectra. This structural assignment method has been widely used on cluster study.[4,31,39,41−46] EA is calculated as the difference between the total energies of the neutral and anion at their respective optimized structures. The theoretical DOS spectra are shifted by setting the HOMO level of the spectra to give the negative of VDE value for the complex. This is called theoretically generalized Koopman theorem (GKT)[47] -shifted DOS.[31] And we know, according to the single electron approximation, the electronic peaks present in the PES spectra correspond to removals of a single electron from different occupied MOs of the anions, so the energy levels are plotted as the stick spectra in the DOS spectra. Because the MOs are dense in the high binding energy area, there are several MOs

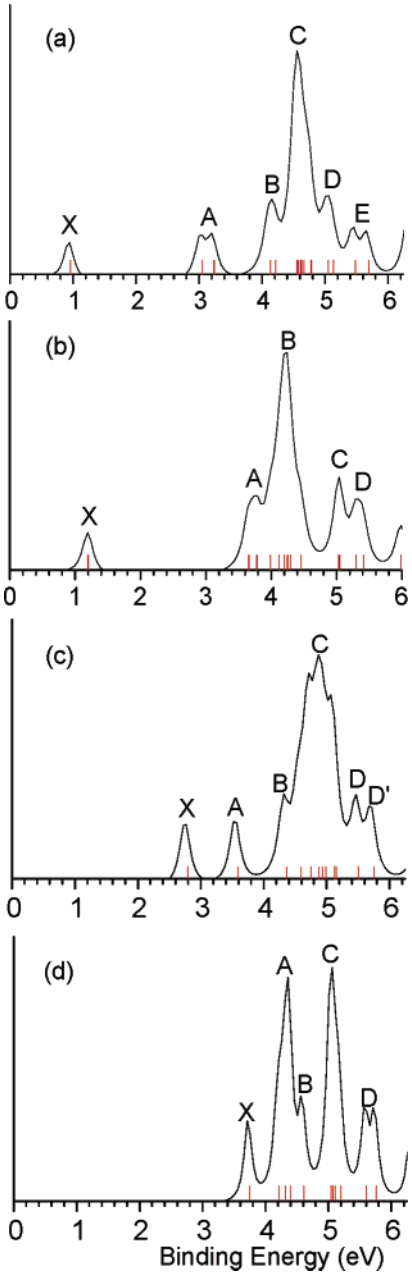

Figure 5. Theoretical generalized Koopman theorem (GKT)-shifted DOS for (a) $AgC_6H_5^-$, (b) $AuC_6H_5^-$, (c) $Ag_2C_6H_5^-$ and (d) $Au_2C_6H_5^-$. In this and subsequent figures, each of the discrete occupied energy levels is broaden by a Lorentzian with a width $\sigma = 0.1$ eV.

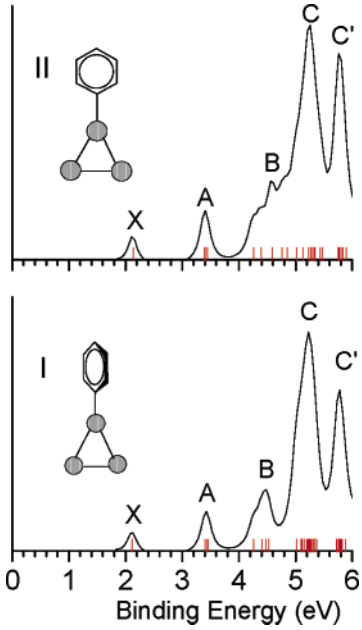

Figure 6. Theoretical generalized Koopman theorem (GKT)-shifted DOS for $Ag_3C_6H_5^-$.

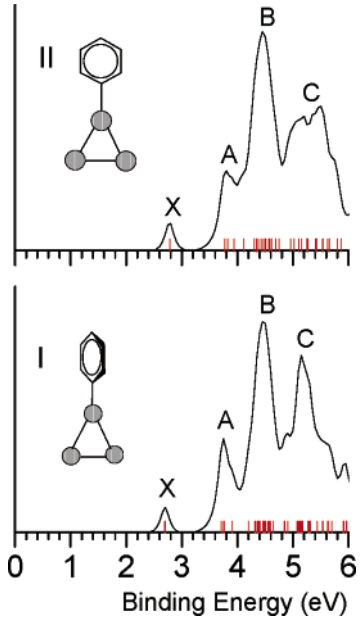

Figure 7. Theoretical generalized Koopman theorem (GKT)-shifted DOS for $Au_3C_6H_5^-$.

in one marked feature and they are assigned in Table 3S and Table 4S. In comparing the DOS spectra and the PES spectra, we focus on the electron binding energy corresponding to each feature, not on the relative intensity, because the relative intensity depends on other factors such as the unknown orbital-dependent photodetachment cross-section.[31]

4.5.1. $AgC_6H_5^-$ and $AuC_6H_5^-$. The planar structure of the C_{2v} symmetry that the phenyl group couples on the metal through the C−M bond is clearly the ground state for both these neutral and anionic complexes. The energy differences between the neutral and anionic structures (corresponding to the calculated EAs) are listed in Table 1. The calculated EAs of AgC_6H_5 and AuC_6H_5 by the relativistic DFT are 0.75 and 0.84 eV, respectively. They are in good agreement with the experimental results 0.66 and 0.80 eV. The DOS spectra of $AgC_6H_5^-$ and $AuC_6H_5^-$ are shown in Figure 5a,b. The HOMO−LUMO energy gap of $AgC_6H_5^-$ and $AuC_6H_5^-$ in DOS spectra is 2.20 and 2.57 eV, respectively. This agrees reasonably well with the experimental gaps of about 2.47 and 2.63 eV. The theoretical VDE of other features (B, C, D, E) for $AgC_6H_5^-$ are 4.13, 4.58, 5.06, and 5.55 eV, corresponding to 4.10, 4.66, 5.14, and 5.60 eV of the features in the PES spectra. As for $AuC_6H_5^-$, VDE of features (X, A, C, D) in the DOS spectra are 1.17, 3.74, 5.03, and 5.32 eV, corresponding to VDE of PES features (X, A, C, D) 1.15, 3.78, 5.15, and 5.40 eV, respectively. Feature B in the DOS spectra of $AuC_6H_5^-$, the VDE of which is 4.25 eV with a strong intensity, corresponds to the two weakly split features B (4.29 eV) and B′ (4.58 eV) in the experimental spectra.

4.5.2. $Ag_2C_6H_5^-$ and $Au_2C_6H_5^-$. These two anionic complexes are closed-shell, there is no large HOMO−LUMO energy gap between the first two features in PES and their EAs are higher

compared with the open-shell anionic structures. The measured EAs of $Ag_2C_6H_5$ and $Au_2C_6H_5$ are 2.66 and 3.52 eV respectively in the PES spectra. The optimized stable structures are similar for the neutral and anionic species, and they are all in a C_{2v} symmetry where the phenyl group binds the metal through a C−M bond and C−M−M (M = Ag, Au) are in a line with the same plane of the phenyl group. The theoretical EAs of $Ag_2C_6H_5$ and $Au_2C_6H_5$ by the relativistic DFT are 2.60 and 3.32 eV, which are consistent with the experimental results. The features A and B of $Ag_2C_6H_5^-$ in the PES spectra are two broad weak features with energy ranges of 3.19−3.64 and 3.83−4.48 eV, corresponding to the features A and B with VDE of 3.53 and 4.31 eV in the DOS spectra. The measured feature C, the VDE of which is 4.84 eV, agrees well with the theoretical feature C with a VDE of 4.88 eV, which contains several excited states because of the congested molecular orbitals that can be seen in the Figure 5c. Feature D in the PES spectra corresponds to the two weak features D and D′ in the DOS spectra, and they are in reasonable agreement taking into account the experimental conditions, such as the photodetachment cross-section. For $Au_2C_6H_5^-$, its EA is the largest one in all complexes that we talk about in this article, so the binding energies of $Au_2C_6H_5$ are in the high energy area with the decreasing experimental resolution. The two weak features A and A′ with VDEs of 4.10 and 4.39 eV in the PES spectra correspond to the strong feature A with a VDE of 4.35 eV, and feature B with a VDE of 4.68 eV agrees well with the same marked feature in the DOS spectra with a VDE of 4.58 eV. The higher binding energy features in the experimental spectra are not clear due to the decreasing resolution and the increasing noise signals. The peak marked C with VDE about 5.14 eV corresponds to the feature C in the DOS spectra with VDE of 5.06 eV. As for feature D in the DOS spectra, it cannot be recognized from the experimental spectra, which needs the higher resolution PES experiment.

4.5.3. $Ag_3C_6H_5^-$ and $Au_3C_6H_5^-$. The theoretical DOS spectra of the five optimized low-lying isomeric structures (I, II, III, VI, VII) for $Ag_3C_6H_5^-$ and seven (I−VII) for $Au_3C_6H_5^-$ are all calculated. For $Ag_3C_6H_5^-$, feature X with a VDE of 2.15 eV in the measured PES spectra matches the theoretical VDE of structures I (2.11 eV) and II (2.10 eV) well in the DOS spectra. There is a large HOMO−LUMO energy gap of about 1.62 eV in the PES spectra; structures I and II best match the gap. Features B of structures I and II are 1.04 and 1.16 eV higher in energy than feature A, and this is consistent with the PES spectra of 0.97 eV. The theoretical EA of structure III with the three metals being in a line is much larger than the measured EA. Feature C in the experimental PES is a broad feature, whereas the feature in this energy scope of all these isomeric structures in the DOS spectra is split. This maybe originates from the effect of experimental factors such as the resolution. Thus, for $Ag_3C_6H_5^-$, it is most likely that the two lowest energy isomers I and II are both present in the products. The experimental data reveal a large HOMO−LUMO energy gap of 1.37 eV for $Au_3C_6H_5^-$. The geometries of isomers IV and V, two C_{2v} structures with the three Au atoms having a big angle, can be ruled out from the PES due to lack of this energy gap. The threshold binding energy of the isomer III is much larger than the threshold value of the measured PES spectra, and the features in the DOS spectra (Figure 4S) of structures VI, VII, with C_s and C_1 symmetries are much different from the experimental PES spectra. However, the two energetically lowest isomers, I and II, with energies close to each other, have a large HOMO−LUMO energy gap of 1.08 and 1.07 eV respectively, which agree reasonably well with the experimental value of 1.37 eV. The broad feature C in the high energy area of about 5.05−5.76 eV in the PES spectra can be explained well by the corresponding features of isomers I and II in the DOS spectra. In the energy scope between peak A and the above-mentioned high binding energy feature C, there are two weak peaks B and B′ in the PES spectra, corresponding to a strong peak B in the DOS spectra of isomers I and II, respectively. According to our comparison, we conclude coexistence of the isomers I and II for $Au_3C_6H_5^-$ in our experimental results.

4.6. Compared with PES of the Pure Coinage Metal Clusters. We mentioned above that the photoelectron spectra of M_m^- and $M_{m-1}C_6H_5^-$ (M = Ag, Au; $m = 2-4$) should have some similarities if their geometry structures are similar because both the M atom and C_6H_5 group contribute a single electron to the bonding orbitals. The experimental PES and theoretical study of the pure Ag_m^- and Au_m^- clusters have been reported.[29−32,48] Here we have also carried out a systemic investigation on the pure coinage metal clusters Ag_m^- and Au_m^- ($m = 2-4$) using the relativistic DFT. The results are consistent with those of the reported data and agree reasonable well with the experimental spectra. Furthermore, this can be a cogent case that these theoretical methods are appropriate for studying the coinage metal clusters.

The ground states of Ag_3^- and Au_3^- are both linear. The cases for Ag_4^- and Au_4^- are a little complicated because of several near energetically low-lying isomers. The rhombus isomer is the most stable structure for Ag_4^- and the DOS spectra features match best with the measured PES, thus it is the dominating structure for the Ag_4^- cluster, which is in agreement with study of V. Bonačić-Koutecký with a CI calculation.[48] Our theoretical work of Au_4^- is similar to that of H. Häkkinen[31] except for some computational details, so the DOS spectra are similar correspondingly. The conclusion is that the second energetically lowest-lying "Y" shape isomer is the predominant structure in the PES experiment of Au_4^- cluster. Therefore, through investigations of the structures for $M_mC_6H_5^-$ complexes and pure coinage metal clusters M_m^-, geometry structures are similar for the following pairs: M_2^- and $MC_6H_5^-$ (M = Ag, Au), both are linear; M_3^- and $M_2C_6H_5^-$ (M = Ag, Au), both are planar linear structures; and Au_4^- with $Au_3C_6H_5^-$, both are planar "Y" shape structures.

The large HOMO−LOMO energy gaps are both present in PES of $AgC_6H_5^-$ and Ag_2^-, and the gap (2.47 eV) of $AgC_6H_5^-$ is bigger than that (about 1.70 eV) of Ag_2^-. Besides, their EAs are close to each other except that EA (0.66 eV) of AgC_6H_5 is a little smaller than that of Ag_2 (1.02 eV), which may be due to the loose π internal orbitals of C_6H_5 group. The obvious difference between them is that excited states of AgC_6H_5 are more complicated due to the congested molecular orbitals in the high binding energy area. Likewise, PESs of Au_2^- and $AuC_6H_5^-$ have large HOMO−LOMO energy gaps, and the gap (2.63 eV) of AuC_6H_5 is larger than that (about 1.90 eV) of Au_2. The EA of Au_2 (1.94 eV) is much larger than that of AuC_6H_5 (0.80 eV); this can be attributed to the obviously stronger relativistic effect of Au_2 than AuC_6H_5. And they both have the congested peaks in binding energy scope of 3.5−5 eV. All of the above discussion can be well understood from the energy level diagrams (Figure 5S) of these neutral species calculated at the anionic geometry. For example, there is a large energy gap between the LUMO ($16a_1$) and HOMO ($15a_1$) of AgC_6H_5, and another between the LUMO ($4\sigma_u$) and HOMO ($4\sigma_g$) of Ag_2. The former one is a little larger than the latter one, which is

consistent with the observed spectra. And the case is the same for Au_2 and AuC_6H_5.

There are two optimized structures of Ag_3^- and Au_3^- for which we calculated the DOS spectra. The triangle one with D_{3h} symmetry has a very large HOMO−LUMO gap, and it is energetically unstable. The linear one is energetically stable, and its DOS spectra agree reasonable well with the measured one. Obviously, the PES of $Ag_2C_6H_5^-$ is more like the spectra of the linear Ag_3^-, but there is some difference too. The EAs of $Ag_2C_6H_5$ and Ag_3 are similar, but the energy gap between the first two features in the PES of $Ag_2C_6H_5^-$ is a little smaller than that of Ag_3^-, and peaks of $Ag_2C_6H_5^-$ in the middle binding energy area are more complicated than Ag_3^-. This can be explained from the energy level diagrams (Figure 5S). We have noted above that there are two possibilities as to the first excited state for the open-shell species, one is electron excitation from the HOMO to the LUMO and the other is from the HOMO−1 to the HOMO. According to Figure 5S, for $Ag_2C_6H_5$, the electron transition from the HOMO ($20a_1$) to the LUMO ($21a_1$) needs much more energy than from the HOMO−1 ($19a_1$) to the HOMO. Thus, the first electronic excited state for $Ag_2C_6H_5$ is assigned as the HOMO−1 to HOMO transition. And the cases are the same for Ag_3, Au_3, and $Au_2C_6H_5$. So we can see from the energy level diagrams that the first excitation energy for Ag_3 is a little bigger than that of $Ag_2C_6H_5$, and the HOMO−2 ($6b_2$) and HOMO−3 ($3a_2$) are near the HOMO−1 of $Ag_2C_6H_5$, whereas the HOMO−2 ($5\sigma_g$) is much lower in energy than the HOMO−1 of Ag_3. This accounts for the difference of the observed spectra between $Ag_2C_6H_5$ and Ag_3. The PES of Au_3^- distinguishes from the PES of Ag_3^- despite their same geometries and valence electrons. The energy gaps of Au_3^- are smaller than those of Ag_3^- and EAs of Au_3^- are much larger than that of Ag_3^-. To take into account of the resolution difference, the PES of $Au_2C_6H_5^-$ is similar to that of Au_3^- and their EAs are almost same too. Therefore, the linear geometries for $Ag_2C_6H_5^-$ and $Au_2C_6H_5^-$ can be affirmed by this comparison.

Ag_4^- is assigned to be a rhombus structure in this work and others.[48] By comparing Figure 2 with Figure 2Se, we can see clearly that the PES spectra of $Ag_3C_6H_5^-$ is much different from the measured spectra of Ag_4^-, which suggests that their geometric structures are different from each other; thus $Ag_3C_6H_5^-$ is not the rhombus or ring form. Furthermore, the PES of $Ag_3C_6H_5^-$ exhibits many more similarities to features of the DOS spectra of the "Y" shape Ag_4^- structure, which implies that the possible structure for $Ag_3C_6H_5^-$ is the "Y" shape, just as the assignment (structure I and II) above in this paper. Au_4^- is assigned as the "Y" shape structure in this and another paper;[31] thus its PES differs much from that of Ag_4^- (Figure 2Se,f), but the PES of Au_4^- is very similar to the PES of $Au_3C_6H_5$. EAs of $Au_3C_6H_5$ and Au_4 are almost the same, and the HOMO−LUMO energy gaps are almost the same too. Moreover, they both display congested peaks in the high binding energy area. Therefore, by this comparison, we can conclude that the structure of $Au_3C_6H_5$ is similar to that of Au_4, which agrees with our above assignment of the coexistence of two C_{2v} isomeric structures (I and II) for $Au_3C_6H_5^-$, which are also "Y" shape structures regardless of the plane of the C_6H_5 group. These similarities between the PESs of Au_4^- and $Au_3C_6H_5^-$ can also be clarified by the energy levels in Figure 5S.

4.7. Orbital Composition and Bonding. We have also analyzed the orbital compositions for the neutral complexes, and the orbital compositions near the HOMO level of these complexes are similar for clusters containing Ag and Au. To verify how these products form, we stress the bonding between the phenyl and the metal fragment. From this point, the bonding or the MOs of these species may be viewed effectively as the fusion of phenyl and metal atom or the metal cluster fragment. As an example, the energy level correlations of $Ag_mC_6H_5$ ($m = 1-3$) from a C_6H_5 group and Ag_m fragment are given in Figure 8 and their MO pictures are given in Figure 9. The MO pictures of C_6H_5, Ag_2 and Ag_3 fragments are shown in Figure 10.

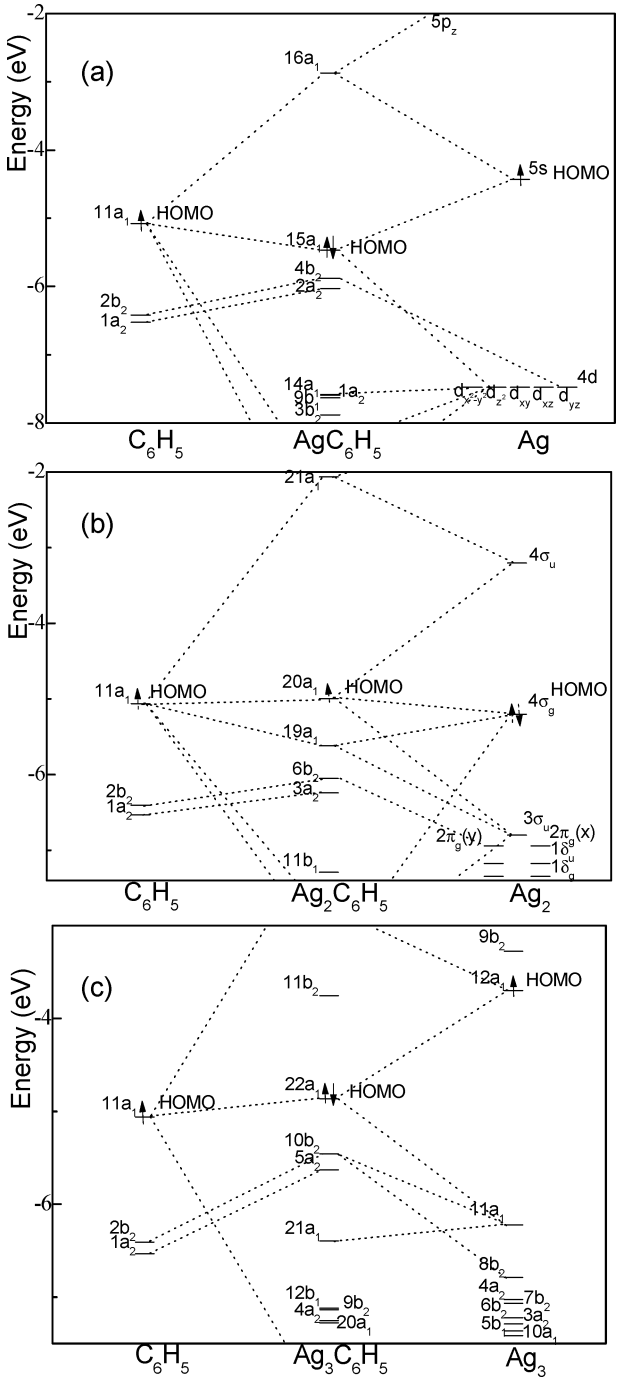

Figure 8. Energy level correlation diagrams of molecular orbitals for (a) AgC_6H_5, (b) $Ag_2C_6H_5$ and (c) $Ag_3C_6H_5$ (structure I). Occupancy is indicated for the HOMO only, and all lower lying levels are doubly occupied.

For AgC_6H_5, the HOMO ($15a_1$) is formed by interaction from 5s and $4d_{z^2}$ of the Ag atom with $11a_1$ of C_6H_5 (C6: $2p_z$) and it is a σ MO for the C−Ag part. The HOMO−1 ($4b_2$) is composed of the $2b_2$ MO of C_6H_5 and $4d_{yz}$ of the Ag atom, and it is a nonbonding MO for the C−Ag part. The HOMO−2 ($2a_2$) is

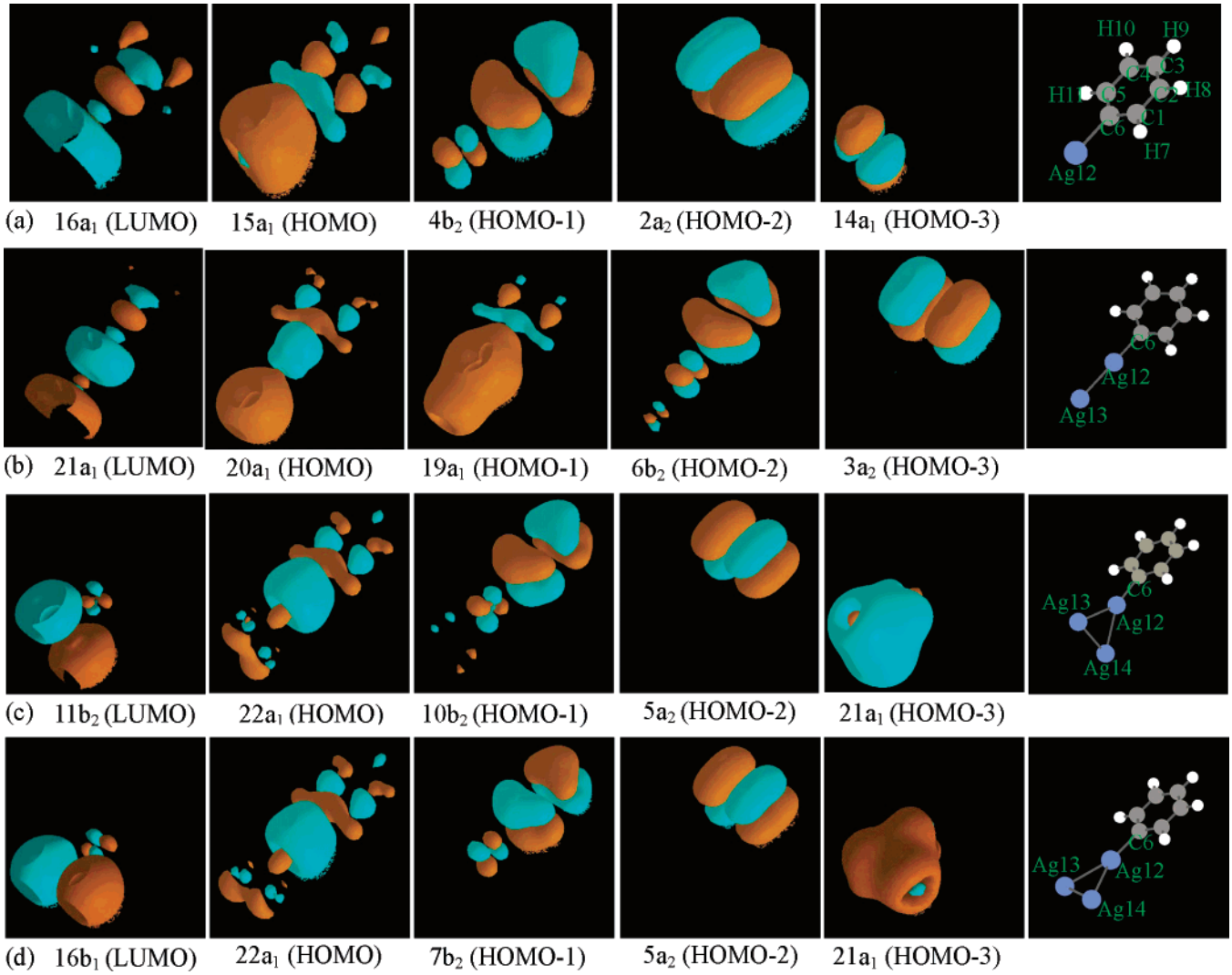

Figure 9. Molecular orbital pictures for (a) AgC_6H_5, (b) $Ag_2C_6H_5$, (c) $Ag_3C_6H_5$ (structure I) and (d) $Ag_3C_6H_5$ (structure II). The last picture in each row is the coordinate sketch of the molecule corresponding to its molecular orbital pictures.

from the $1a_2$ MO of C_6H_5 formed by $2p_y$ atomic orbitals of carbon atoms, and the HOMO−3 ($14a_1$) mainly comes from $4d_{x^2-y^2}$ of the Ag atom. And the inner MOs are also nonbonding MOs for the C−Ag part. Therefore, the Ag atom and the phenyl group bind together by the σ bond that the 5s and $4d_{z^2}$ orbitals of Ag atom hybridized, and then they bond with the $2p_z$ orbital of the nearest C6 atom.

As for $Ag_2C_6H_5$, by analysis of the orbital data and pictures, 5s of the Ag13 atom and $5p_z$, $4d_{z^2}$ of the Ag12 atom are combined to form MOs; then they interact with $2p_z$ of the C6 atom to make a σ bond in the HOMO of $Ag_2C_6H_5$. As from MOs of the fragment, the HOMO of this complex is combined with $11a_1$ of the C_6H_5 group and $4\sigma_u$, $4\sigma_g$, and $3\sigma_u$ of the Ag_2 group. In the HOMO−1, 5s and $4d_{z^2}$ of the Ag12 atom are combined with 5s of the Ag13 atom, and then they interact with the $2p_z$ atomic orbital of the C6 atom mainly to compose the σ bond including Ag13−Ag12−C6. From the fragment's point, the HOMO−1 is combined with $11a_1$ of C_6H_5 and $4\sigma_g$ and $3\sigma_u$ of the Ag_2 group. The HOMO−2, HOMO−3 and inner MOs are all nonbonding MOs for the C−M part. Consequently, the Ag_2 fragment couples to the phenyl fragment through the C−M σ bond.

There are two possible isomeric structures of $Ag_3C_6H_5^-$, so we investigate the MOs and bonding for the two isomers I and II of the neutral AgC_6H_5. In structures I and II, their MOs near the HOMO are similar, so the energy level correlation is only given for structure I in Figure 8. Their HOMOs are both $22a_1$, which can be seen as combinations of $11a_1$ of the phenyl group and $12a_1$ of the Ag_3 group, and the Ag−C is a σ bond formed mainly from 5s and $4d_{z^2}$ of the Ag12 atom interacting with $2p_z$ of the C6 atom. Their HOMO−2 and HOMO−3 are similar as well, which are both $5a_2$ and $21a_1$, simply coming from $1a_2$ of C_6H_5 and from $11a_1$ of the Ag_3 group, respectively. The HOMO−1s of these two structures are a little different, structure II ($7b_2$) is composed of $2b_2$ of C_6H_5 and $4d_{yz}$ of the Ag12 atom; for structure I ($10b_2$), there is also a little contribution from 5s of the Ag13 and Ag14 atoms. For the inner MOs of these two structures, analyzed by the calculated data, there is no contribution or little to the Ag−C bond, such as in structure I where HOMO−17 is a very weak π orbital and HOMO−22 is a very weak σ orbital for the Ag−C part. Thus, we conclude that in $Ag_3C_6H_5$, the Ag_3 cluster connects to the phenyl group with the C−M σ bond.

5. Conclusions

Phenyl-coinage metal (Ag, Au) complexes with 1−3 metal atoms are produced from laser vaporization. A combined experimental and theoretical effort is made to elucidate the bindings, geometric and electronic structures of these species. EAs of $M_mC_6H_5$ (M = Ag and Au; m = 1−3) are obtained

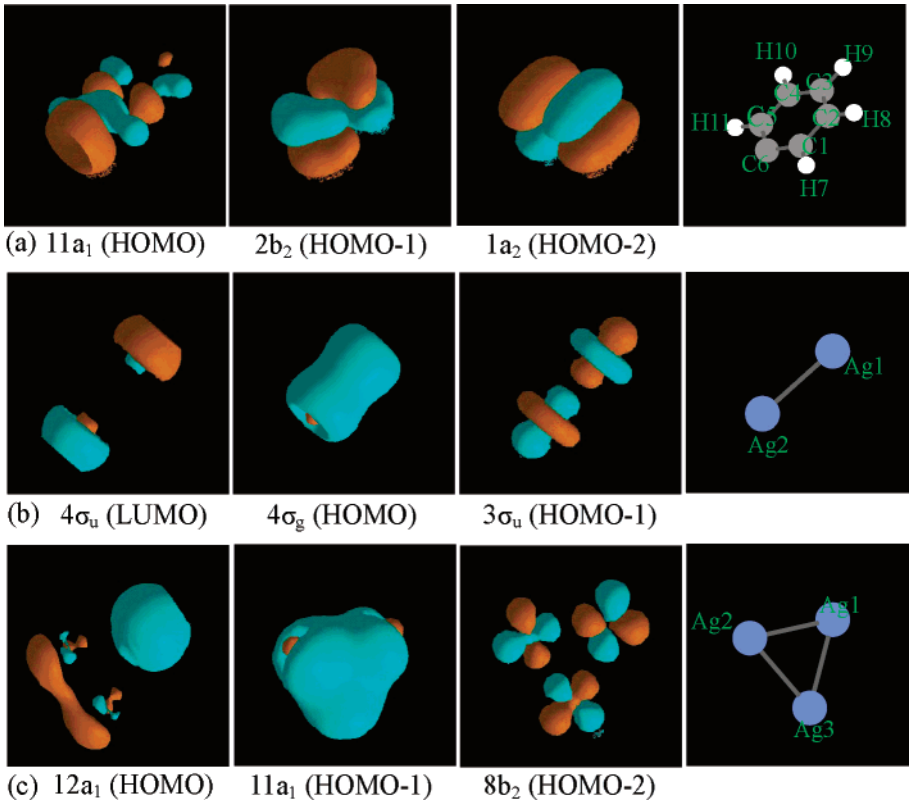

Figure 10. Molecular orbital pictures for fragments (a) C_6H_5, (b) Ag_2 and (c) Ag_3. The last picture in each row is the coordinate sketch of the molecule corresponding to its molecular orbital pictures.

from the photoelectron spectra at both 308 and 193 nm photons and show odd−even alternation. For each species, we conclude the most possible structures by comparison of the measured spectra with the theoretical EAs and simulated DOS spectra calculated by the relativistic DFT. The good agreement between the calculated results and the experimental spectra suggests that $M_mC_6H_5^-$ (M = Ag and Au; m = 1−3) present in our experiment possessing C_{2v} ground-state structure, and the complexes with three metal atoms have two isomeric structures in the products. The comparisons between the observed spectra of these complexes and the pure coinage metal clusters suggest that the phenyl acts like an additional metal atom in the clusters, and also support the structures assigned for these complexes. The MO analysis of these species and their component fragments indicates that the phenyl group binds perpendicularly on metal clusters through C−M σ bond.

Acknowledgment. We gratefully acknowledge the support of the National Natural Science Foundation of China under Grant 20203020. We thank Professor Qihe Zhu and Zhen Gao for their original design and assembly of the experimental apparatus.

Supporting Information Available: Figure 1S, Table 1S and Figure 2S report experimental spectra and theoretical results for pure coinage metal clusters. Table 2S lists total and relative energies and EAs. Table 3S and 4S list the VDE of the detachment features in PES spectra, theoretical DOS spectra and molecular orbital assignment for $M_3C_6H_5^-$ (M = Ag and Au; m = 1−3). Figure 3S and 4S show simulated DOS spectra of other isomeric structures. Figure 5S reports the energy level diagrams for neutral species calculated at their respectively lowest-lying anionic structure. This material is available free of charge via the Internet at http://pubs.acs.org.

References and Notes

(1) Landman, U.; Luedtke, W. D.; Burnham, N. A.; Colton, R. J. *Science* **1990**, *248*, 454.
(2) Häkkinen, H.; Barnett, R. N.; Scherbakov, A. G.; Landman, U. *J. Phys. Chem. B* **2000**, *104*, 9063.
(3) Cleveland, C. L.; Landman, U.; Schaaff, T. G.; Shafigullin, M. N.; Stephens, P. W.; Whetten, R. L. *Phys. Rev. Lett.* **1997**, *79*, 1873.
(4) Häkkinen, H.; Barnett, R. N.; Landman, U. *Phys. Rev. Lett.* **1999**, *82*, 3264.
(5) Yoon, B.; Häkkinen, H.; Landman, U.; Worz, A. S.; Antonietti, J. M.; Abbet, S.; Judai, K.; Heiz, U. *Science* **2005**, *307*, 403.
(6) Sanchez, A.; Abbet, S.; Heiz, U.; Schneider, W. D.; Häkkinen, H.; Barnett, R. N.; Landman, U. *J. Phys. Chem. A* **1999**, *103*, 9573.
(7) Häkkinen, H.; Landman, U. *J. Am. Chem. Soc.* **2001**, *123*, 9704.
(8) Kimble, M. L.; Castleman, A. W.; Mitric, R.; Burgel, C.; Bonacic-Koutecky, V. *J. Am. Chem. Soc.* **2004**, *126*, 2526.
(9) Hagen, J.; Socaciu, L. D.; Le Roux, J.; Popolan, D.; Bernhardt, T. M.; Woste, L.; Mitric, R.; Noack, H.; Bonacic-Koutecky, V. *J. Am. Chem. Soc.* **2004**, *126*, 3442.
(10) Socaciu, L. D.; Hagen, J.; Bernhardt, T. M.; Woste, L.; Heiz, U.; Hakkinen, H.; Landman, U. *J. Am. Chem. Soc.* **2003**, *125*, 10437.
(11) Wallace, W. T.; Whetten, R. W. *J. Am. Chem. Soc.* **2002**, *124*, 7499.
(12) Stolcic, D.; Fischer, M.; Ganteför, G.; Kim, Y. D.; Sun, Q.; Jena, P. *J. Am. Chem. Soc.* **2003**, *125*, 2848.
(13) Brolo, A. G.; Irish, D. E.; Smith, B. D. *J. Mol. Struct.* **1997**, *405*, 29.
(14) Xi, M.; Bent, B. E. *Surf. Sci.* **1992**, *278*, 19.
(15) Yang, M. X.; Xi, M.; Yuan, H.; Bent, B. E.; Stevens, P.; White, J. M. *Surf. Sci.* **1995**, *341*, 9.
(16) Syomin, D.; Kim, J.; Koel, B. E.; Ellison, G. B. *J. Phys. Chem. B* **2001**, *105*, 8387.
(17) Fanta, P. E. *Chem. Rev.* **1964**, *64*, 613.
(18) Hosshino, K.; Kurikawa, T.; Takeda, H.; Nakajima, A.; Kaya, K. *J. Phys. Chem.* **1995**, *99*, 3035.
(19) Kurikawa, T.; Hirano, M.; Takeda, H.; Yagi, K.; Hoshino, K.; Nakajima, A.; Kaya, K. *J. Phys. Chem.* **1995**, *99*, 16429.
(20) Kurkawa, T.; Takeda, H.; Hiranok, M.; Judai, K.; Arita, T.; Nagao, S.; Nakajima, A.; Kaya, K. *Organometallics* **1999**, *18*, 1430.
(21) Gerhards, M.; Thomas, O. C.; Nilles, J. M.; Zheng, W.; Bowen, K. H. *J. Chem. Phys.* **2002**, *116*, 10247.
(22) Xing, X. P.; Liu, H. T.; Tang, Z. C. *PhysChemComm* **2003**, *6*, 32.

(23) Xing, X. P.; Tian, Z. X.; Liu, H. T.; Tang, Z. C. *J. Phys. Chem. A* **2003**, *107*, 8484.
(24) Zheng, W.; Nilles, J. M.; Thomas, O. C.; Bowen, K. H. *J. Chem. Phys.* **2005**, *122*, 44306.
(25) Zheng, W.; Nilles, J. M.; Thomas, O. C.; Bowen, K. H. *Chem. Phys. Lett.* **2005**, *401*, 266.
(26) Pandey, R.; Rao, B. K.; Purusottam, J.; Blanco, M. A. *J. Am. Chem. Soc.* **2001**, *123*, 3799.
(27) Rao, B. K.; Jena, P. *J. Chem. Phys.* **2002**, *117*, 5234.
(28) Kandalam, A. K.; Rao, B. K.; Jena, P. *J. Chem. Phys.* **2004**, *120*, 10414.
(29) Ho, J.; Ervin, K. M.; Lineberger, W. C. *J. Chem. Phys.* **1990**, *93*, 6987.
(30) Taylor, K. J.; Pettiette-Hall, C. L.; Cheshnovsky, O.; Smalley, R. E. *J. Chem. Phys.* **1992**, *96*, 3319.
(31) Häkkinen, H.; Yoon, B.; Landman, U.; Li, X.; Zhai, H. J.; Wang, L. S. *J. Phys. Chem. A* **2003**, *107*, 6168.
(32) Handschuh, H.; Cha, C.-Y.; Bechthold, P. S.; Ganteför, G.; Eberhardt, W. *J. Chem. Phys.* **1995**, *102*, 6406.
(33) Buckart, S.; Ganteför, G.; Kim, Y. D.; Jena, P. *J. Am. Chem. Soc.* **2003**, *125*, 14205.
(34) Xing, X. P.; Tian, Z. X.; Liu, P.; Gao, Z.; Zhu, Q. H.; Tang, Z. C. *Chin. J. Chem. Phys.* **2002**, *15*, 83.
(35) Xing, X. P.; Liu, H. T.; Sun, S. T.; Cao, Y. L.; Tang, Z. C. *Chin. J. Chem. Phys.* **2004**, *17*, 321.
(36) Perdew, J. P.; Wang, Y. *Phys. Rev. B* **1992**, *45*, 13244.
(37) Lenthe, E. V.; Baerends, E. J.; Snijders, J. G. *J. Chem. Phys.* **1993**, *99*, 4597.
(38) Vrije Universiteit, ADF 2002, SCM, Theoretical Chemistry, Amsterdam, Netherland (www.Scm.com).
(39) Li, J.; Li, X.; Zhai, H. J.; Wang, L. S. *Science* **2003**, *299*, 864.
(40) Antes, I.; Frenking, G. *Organometallics* **1995**, *14*, 4263.
(41) Häkkinen, H.; Moseler, M.; Landman, U. *Phys. Rev. Lett.* **2002**, *89*, 33401.
(42) Li, X.; Kiran, B.; Li, J.; Zhai, H. J.; Wang, L. S. *Angew. Chem., Int. Ed.* **2002**, *41*, 4786.
(43) Wang, L. S.; Wang, X. B.; Wu, H.; Cheng, H. *J. Am. Chem. Soc.* **1998**, *120*, 6556.
(44) Castro, M.; Liu, S. R.; Zhai, H. J.; Wang, L. S. *J. Chem. Phys.* **2003**, *118*, 2116.
(45) Häkkinen, H.; Moseler, M.; Kostko, O.; Morgner, N.; Hoffmann, M. A.; Issendorff, B. V. *Phys. Rev. Lett.* **2004**, *93*, 93401.
(46) Wang, J. L.; Wang, G. H.; Zhao, J. J. *Phys. Rev. B* **2002**, *66*, 35418.
(47) Tozer, D. J.; Handy, N. C. *J. Chem. Phys.* **1998**, *108*, 2545.
(48) Bonačić-Koutecký, V.; Češpiva, L.; Fantucci, P.; Pittner, J.; Koutecký, J. *J. Chem. Phys.* **1994**, *100*, 490.

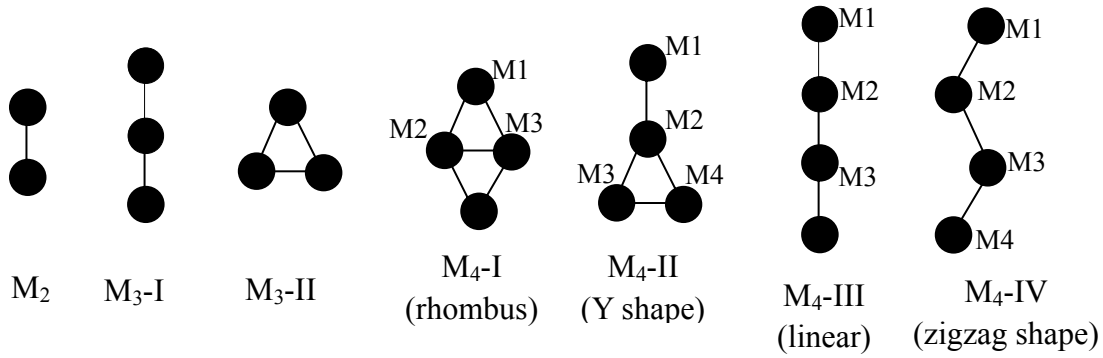

Figure 1S. Optimized structures for neutral and anionic pure coinage metal clusters (M=Ag and Au).

Table 1S. Structural and Energetic Characteristics for Neutral and Anionic Pure Coinage Metal Clusters.

	isomer	Point group	R_{M1-M2} (Å)	R_{M2-M3} (Å)	$\theta_{M2-M3-M4}$ (degree)	ΔE^a (eV)	EA (eV)	
							cal.	exp.[b]
Ag_2		$D_{\infty h}$	2.56			0.00	1.03	1.02
Ag_2^-		$D_{\infty h}$	2.68			0.00		
Ag_3	I	$D_{\infty h}$	2.62			0.00	2.34	2.32
	II	D_{3h}	2.68			0.12	1.24	
Ag_3^-	I	$D_{\infty h}$	2.68			0.00		
	II	D_{3h}	2.75			1.12		
Ag_4	I	D_{2h}	2.73	2.60		0.00	1.68	1.51
	II	C_{2v}	2.57	2.73	61.7	0.21	1.78	
	III	$D_{\infty h}$	2.58	2.68		0.64	2.21	
Ag_4^-	I	D_{2h}	2.72	2.76		0.00		
	II	C_{2v}	2.68	2.68	60.0	0.11		
	III	$D_{\infty h}$	2.68	2.68		0.10		
Au_2		$D_{\infty h}$	2.53			0.00	1.91	1.94
Au_2^-		$D_{\infty h}$	2.68			0.00		
Au_3	I	$D_{\infty h}$	2.58			0.00	3.62	3.67
	II	D_{3h}	2.68			0.02	2.09	
Au_3^-	I	$D_{\infty h}$	2.59			0.00		
	II	D_{3h}	2.73			1.55		
Au_4	I	D_{2h}	2.68	2.68		0.00	2.50	2.60
	II	C_{2v}	2.53	2.68	60.9	0.05	2.67	
	III	$D_{\infty h}$	2.56	2.65		0.89	3.46	
	IV	C_{2h}	2.53	2.59	126.6	0.43	3.07	
Au_4^-	I	D_{2h}	2.71	2.76		0.14		
	II	C_{2v}	2.57	2.69	59.8	0.02		
	III	$D_{\infty h}$	2.60	2.62		0.07		
	IV	C_{2h}	2.58	2.60	154.8	0.00		

[a]ΔE is the difference of cluster energy relative to the correspondingly lowest-lying structure. [b]Reference 29

Figure 2S. Experimental spectra[a,b] and theoretical DOS spectra for (a) Ag_2^-, (b) Au_2^-, (c) Ag_3^-, (d) Au_3^-, (e) Ag_4^- and (f) Au_4^-. [a]Reference 33, [b]Reference 31

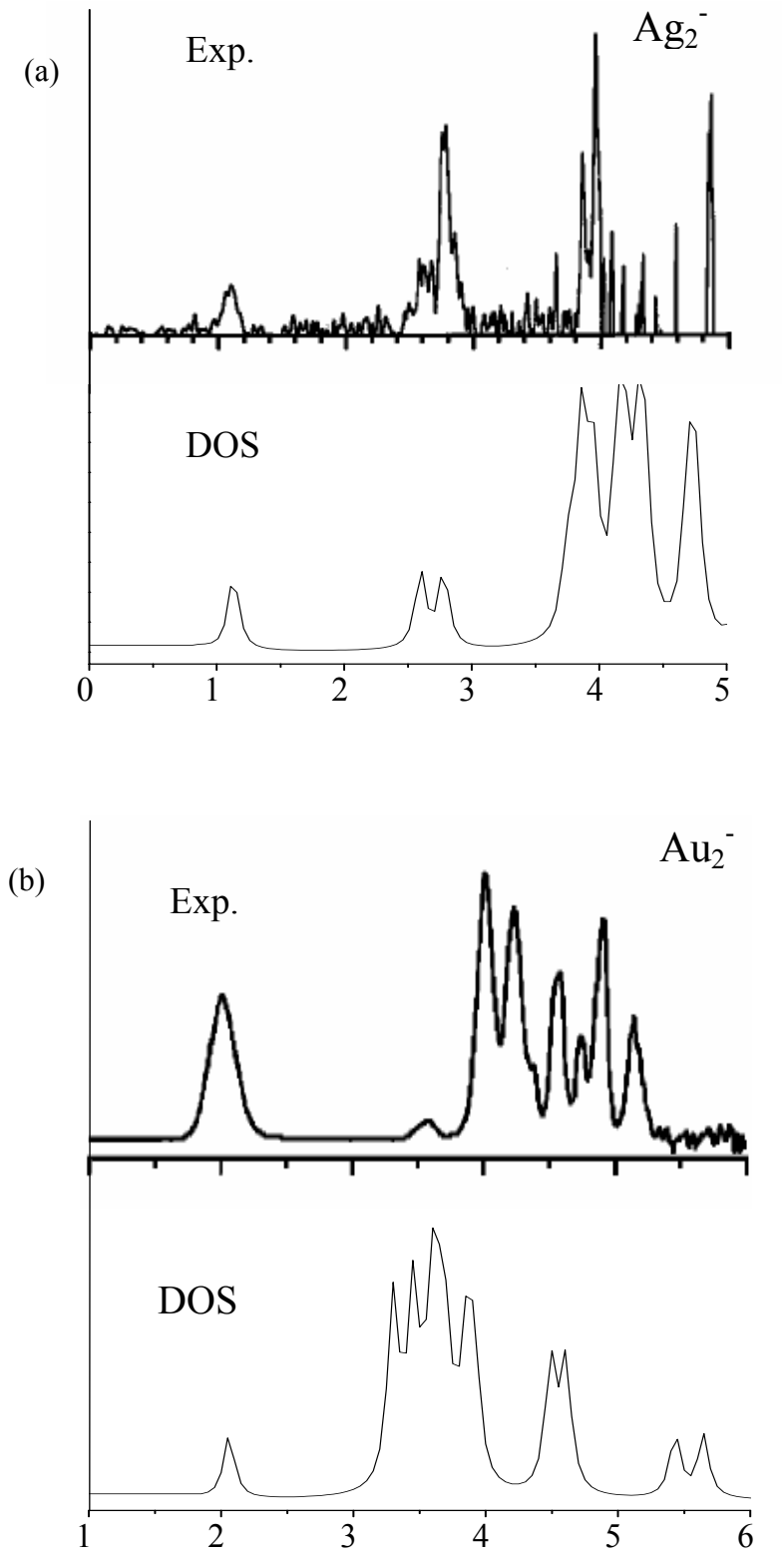

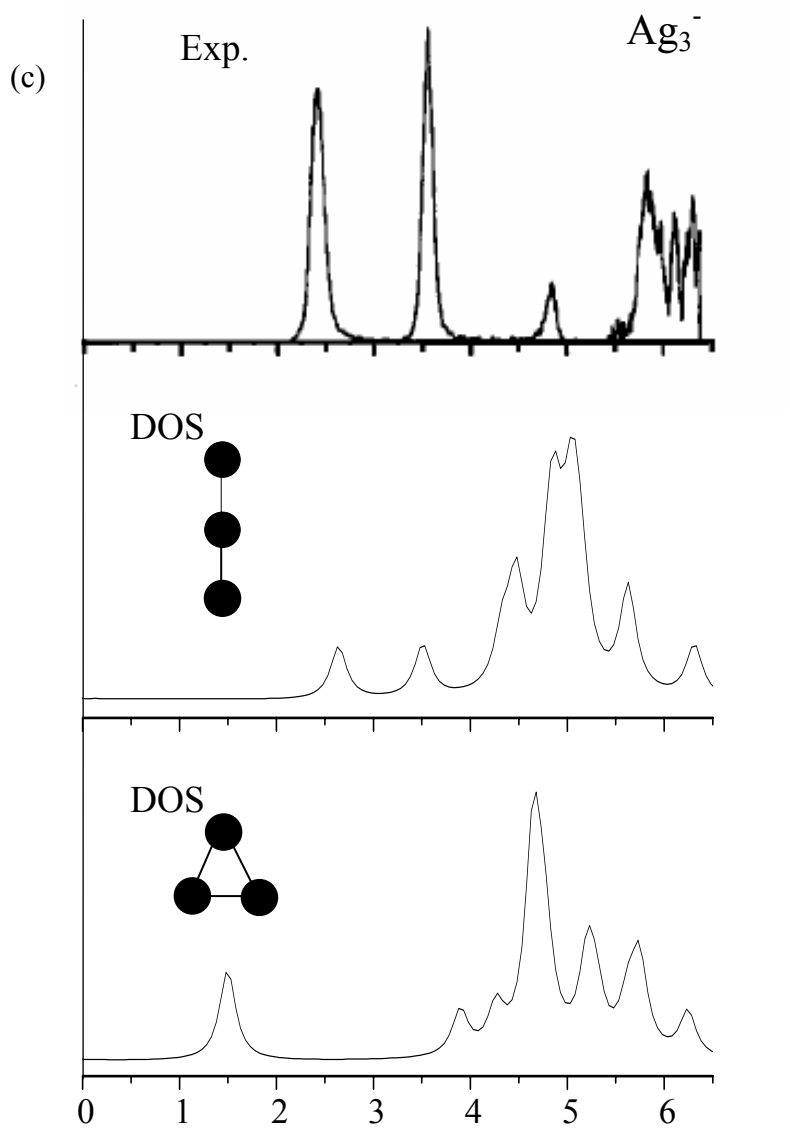
(c)
Exp.
Ag_3^-
DOS
DOS
0
1
2
3
4
5
6

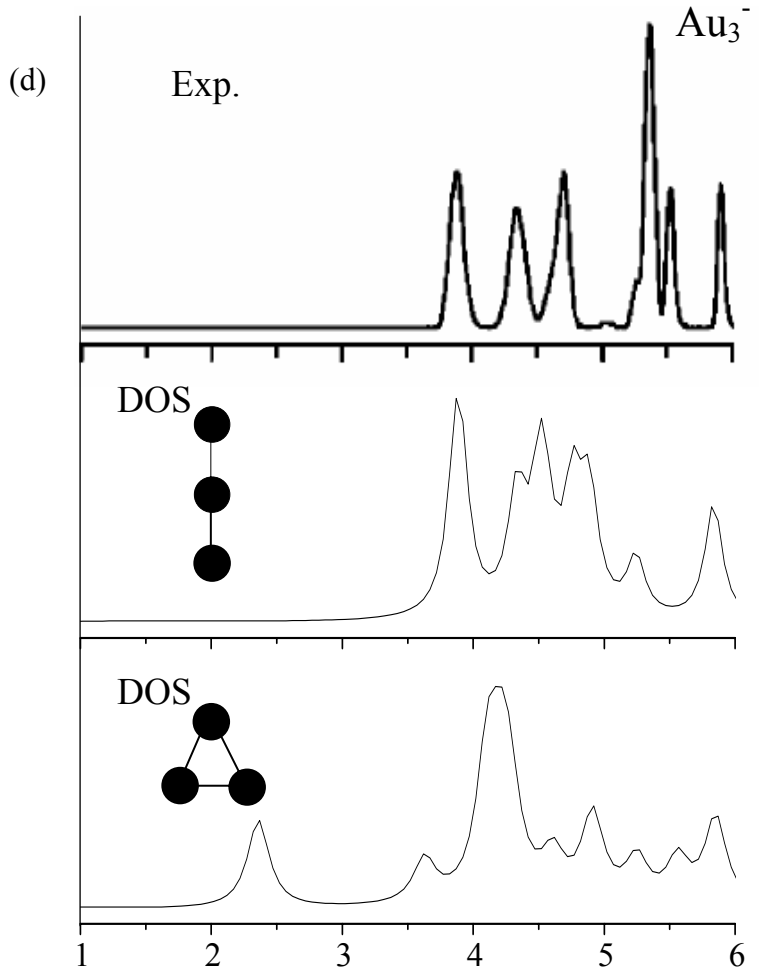
(d)
Exp.
Au_3^-
DOS
DOS
1
2
3
4
5
6

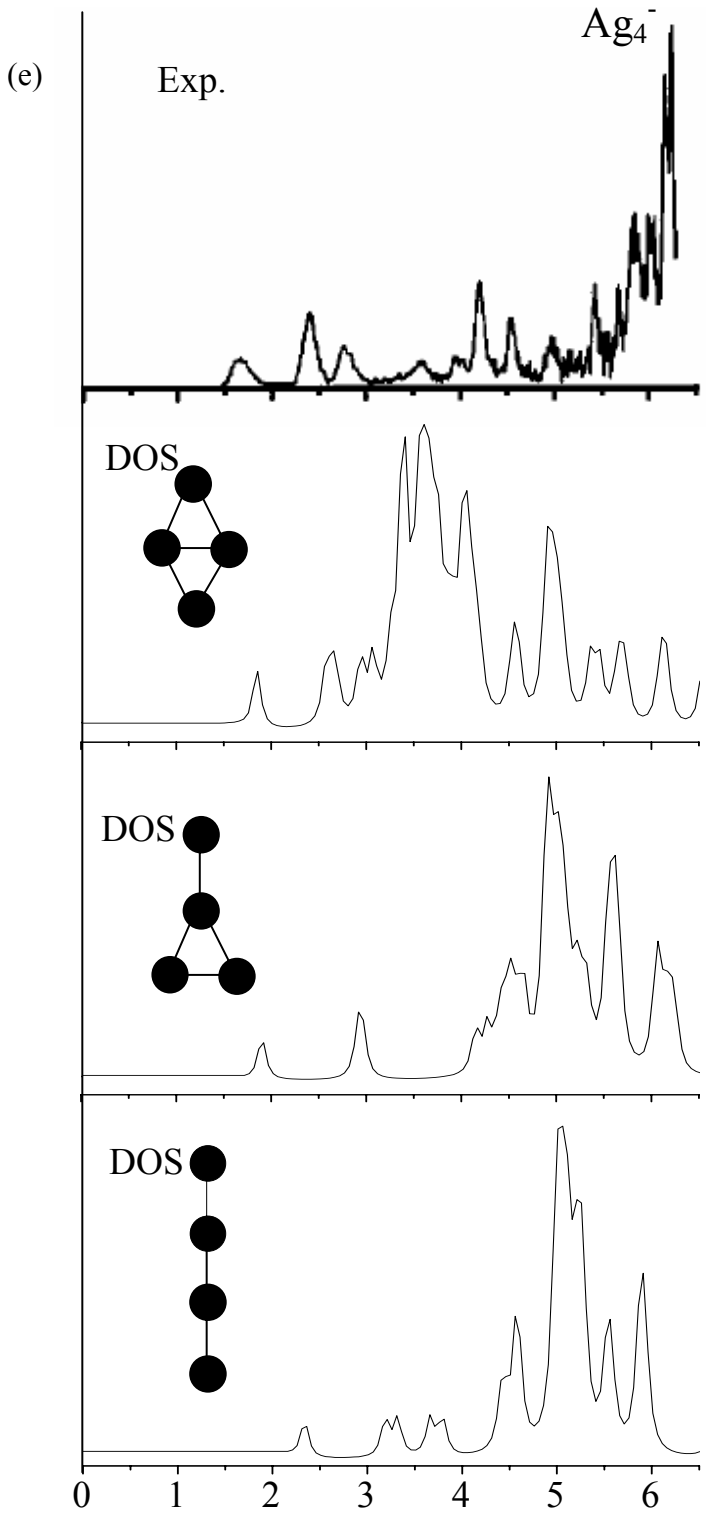
(e)
Exp.
Ag_4^-
DOS
DOS
DOS
0
1
2
3
4
5
6

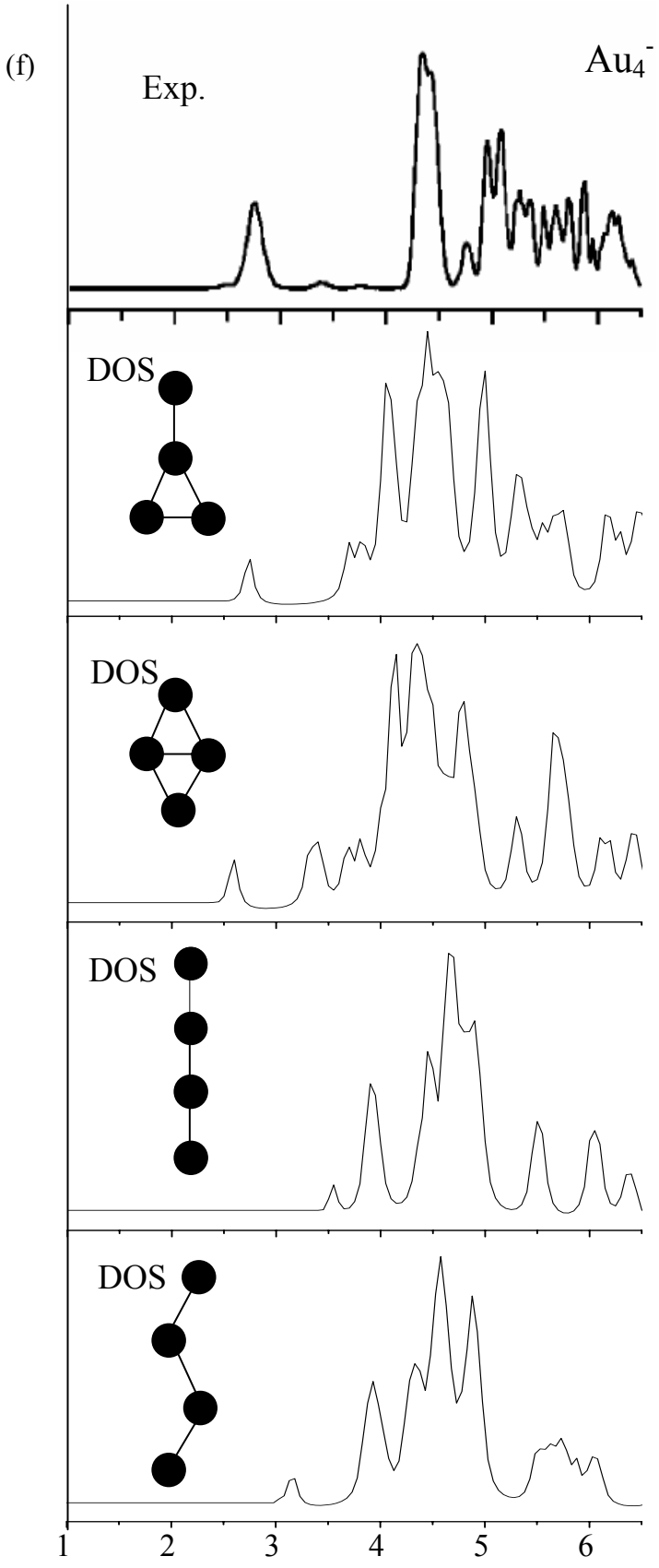
(f)
Exp.
Au_4^-
DOS
DOS
DOS
DOS
1
2
3
4
5
6

Table 2S. Total Energies, Relative Energies and Calculated EA for Complexes of $M_mC_6H_5$ (M= Ag and Au; m=1-3).

	isomer	energy (eV)	ΔE^a (eV)	EA (eV) cal.
AgC_6H_5		-72.889	0.00	0.75
$AgC_6H_5^-$		-73.635	0.00	
$Ag_2C_6H_5$		-73.883	0.00	2.60
$Ag_2C_6H_5^-$		-76.480	0.00	
$Ag_3C_6H_5$	I	-76.179	0.00	1.82
	II	-76.150	0.03	1.84
	III	-75.463	0.72	2.39
	VI	-76.129	0.05	1.72
	VII	-76.148	0.03	1.70
$Ag_3C_6H_5^-$	I	-78.001	0.00	
	II	-77.995	0.01	
	III	-77.854	0.15	
	VI	-77.851	0.15	
	VII	-77.847	0.15	
AuC_6H_5		-73.661	0.00	0.84
$AuC_6H_5^-$		-74.504	0.00	
$Au_2C_6H_5$		-75.047	0.00	3.32
$Au_2C_6H_5^-$		-78.366	0.00	
$Au_3C_6H_5$	I	-77.605	0.00	2.57
	II	-77.504	0.10	2.65
	III	-76.864	0.74	3.22
	IV	-76.871	0.73	2.55
	V	-76.788	0.82	2.76
	VI	-77.462	0.14	2.64
	VII	-77.487	0.12	2.64
$Au_3C_6H_5^-$	I	-80.177	0.00	
	II	-80.153	0.02	
	III	-80.081	0.10	
	IV	-79.418	0.76	
	V	-79.551	0.63	
	VI	-80.097	0.08	
	VII	-80.129	0.05	

[a]ΔE is the difference of cluster energy relative to the correspondingly lowest lying structure.

Table 3S**.** Vertical Detachment Energies of the Detachment Features in PES Spectra and Theoretical DOS Spectra of $M_mC_6H_5^-$ (M= Ag and Au; m=1, 2).

		VDE (eV)		assignment[b]			VDE (eV)		assignment[b]
		exp.[a]	cal.				exp.[a]	cal.	
$AgC_6H_5^-$	X	0.94	0.93	$(16a_1)^\alpha$	$AuC_6H_5^-$	X	1.15	1.17	$(18a_1)^\alpha$
	A	3.41	3.13	$(15a_1)^\beta$		A	3.78	3.74	$(17a_1)^\beta$
				$(15a_1)^\alpha$					$(17a_1)^\alpha$
	B	4.10	4.13	$(4b_2)^\beta$		B	4.29	4.25	$(6b_2)^\beta$
				$(4b_2)^\alpha$					$(6b_2)^\alpha$
	C	4.66	4.58	$(9b_1)^\beta$					$(3a_2)^\beta$
				$(2a_2)^\beta$					$(16a_1)^\beta$
				$(14a_1)^\beta$					$(3a_2)^\alpha$
				$(2a_2)^\alpha$					$(16a_1)^\alpha$
				$(14a_1)^\alpha$					$(11b_1)^\beta$
				$(9b_1)^\alpha$					$(11b_1)^\alpha$
				$(1a_2)^\beta$					
				$(1a_2)^\alpha$		B'	4.58		
	D	5.14	5.06	$(3b_2)^\beta$		C	5.15	5.03	$(2a_2)^\beta$
				$(3b_2)^\alpha$					$(2a_2)^\alpha$
	E	5.60	5.55	$(13a_1)^\beta$		D	5.40	5.32	$(5b_2)^\beta$
				$(13a_1)^\alpha$					$(5b_2)^\alpha$
$Ag_2C_6H_5^-$	X	2.88	2.76	$20a_1$	$Au_2C_6H_5^-$	X	3.72	3.71	$24a_1$
	A	3.19-3.64	3.53	$19a_1$		A	4.10	4.35	$10b_2$
	B	3.83-4.48	4.31	$6b_2$					$15b_1$
	C	4.84	4.88	$11b_1$					$5a_2$
				$3a_2$					$23a_1$
				$18a_1$		A'	4.39		
				$17a_1$					
				$5b_2$		B	4.68	4.58	$22a_1$
				$2a_2$		C	5.14	5.06	$21a_1$
				$16a_1$					$4a_2$
				$1a_2$					$20a_1$
	D	5.48	5.46	$10b_1$					$9b_2$
	D'		5.68	$4b_2$		D		5.66	$3a_2$
									$14b_1$

[a] The uncertainty for the experimental VDE is ±0.05 eV.

[b] The assignment is the orbital of anion from which the electron detached belong to each feature, one to one corresponding to the stick spectra in the DOS spectra, and the orbitals are listed from low to high binding energy.

Table 4S. Vertical Detachment Energies of the Detachment Features in PES Spectra and Theoretical DOS Spectra of $M_3C_6H_5^-$ (M= Ag and Au).

	VDE (eV)			assignment[b]			VDE (eV)			assignment[b]	
		cal.						cal.			
	exp.[a]	isomer I	isomer II	isomer I	isomer II		exp.[a]	isomer I	isomer II	isomer I	isomer II
		$Ag_3C_6H_5^-$						$Au_3C_6H_5^-$			
X	2.15	2.11	2.10	$(11b_2)^\alpha$	$(16b_1)^\alpha$	X	2.69	2.69	2.76	$(17b_2)^\alpha$	$(22b_1)^\alpha$
A	3.77	3.44	3.42	$(22a_1)^\beta$	$(22a_1)^\beta$	A	4.06	3.77	3.83	$(28a_1)^\beta$	$(28a_1)^\beta$
				$(22a_1)^\alpha$	$(22a_1)^\alpha$					$(28a_1)^\alpha$	$(28a_1)^\alpha$
B	4.74	4.48	4.58	$(21a_1)^\beta$	$(21a_1)^\beta$					$(16b_2)^\beta$	$(21b_1)^\beta$
				$(21a_1)^\alpha$	$(21a_1)^\alpha$					$(16b_2)^\alpha$	$(21b_1)^\alpha$
				$(10b_2)^\beta$	$(7b_2)^\beta$	B	4.38	4.46	4.48	$(9a_2)^\beta$	$(9a_2)^\beta$
				$(10b_2)^\alpha$	$(7b_2)^\alpha$					$(15b_2)^\beta$	$(12b_2)^\beta$
C	5.13-5.84	5.21	5.24	$(5a_2)^\beta$	$(15b_1)^\beta$					$(9a_2)^\alpha$	$(12b_2)^\alpha$
				$(5a_2)^\alpha$	$(15b_1)^\alpha$					$(14b_2)^\beta$	$(20b_1)^\beta$
				$(9b_2)^\beta$	$(5a_2)^\beta$					$(8a_2)^\beta$	$(9a_2)^\alpha$
				$(9b_2)^\alpha$	$(5a_2)^\alpha$					$(8a_2)^\alpha$	$(8a_2)^\beta$
				$(4a_2)^\beta$	$(14b_1)^\beta$					$(15b_2)^\alpha$	$(19b_1)^\beta$
				$(8b_2)^\beta$	$(4a_2)^\beta$					$(14b_2)^\alpha$	$(8a_2)^\alpha$
				$(12b_1)^\beta$	$(3a_2)^\beta$					$(17b_1)^\beta$	$(20b_1)^\alpha$
				$(4a_2)^\alpha$	$(14b_1)^\alpha$					$(17b_1)^\alpha$	$(19b_1)^\alpha$
				$(3a_2)^\beta$	$(4a_2)^\alpha$					$(27a_1)^\beta$	$(27a_1)^\beta$
				$(12b_1)^\alpha$	$(13b_1)^\beta$					$(27a_1)^\alpha$	$(27a_1)^\alpha$
				$(8b_2)^\alpha$	$(3a_2)^\alpha$	B'	4.64				
				$(3a_2)^\alpha$	$(20a_1)^\beta$					$(26a_1)^\beta$	$(26a_1)^\beta$
				$(7b_2)^\beta$	$(20a_1)^\alpha$	C	5.05-5.76	5.16	5.51	$(26a_1)^\alpha$	$(26a_1)^\alpha$
				$(20a_1)^\beta$	$(13b_1)^\alpha$					$(13b_2)^\beta$	$(11b_2)^\beta$
				$(20a_1)^\alpha$	$(6b_2)^\beta$					$(13b_2)^\alpha$	$(11b_2)^\alpha$
				$(7b_2)^\alpha$	$(6b_2)^\alpha$					$(7a_2)^\beta$	$(7a_2)^\beta$
C'		5.78	5.77	$(11b_1)^\beta$	$(19a_1)^\beta$					$(7a_2)^\alpha$	$(7a_2)^\alpha$
				$(19a_1)^\beta$	$(2a_2)^\beta$					$(16b_1)^\beta$	$(6a_2)^\beta$
				$(2a_2)^\beta$	$(5b_2)^\beta$					$(16b_1)^\alpha$	$(6a_2)^\alpha$
				$(19a_1)^\alpha$	$(2a_2)^\alpha$					$(6a_2)^\beta$	$(10b_2)^\beta$
				$(11b_1)^\alpha$	$(19a_1)^\alpha$					$(6a_2)^\alpha$	$(25a_1)^\beta$
				$(2a_2)^\alpha$	$(18a_1)^\beta$					$(25a_1)^\beta$	$(10b_2)^\alpha$
				$(18b_1)^\beta$	$(5b_2)^\alpha$					$(25a_1)^\alpha$	$(25a_1)^\alpha$
				$(18b_1)^\alpha$	$(18a_1)^\alpha$					$(24a_1)^\beta$	$(24a_1)^\beta$
										$(24a_1)^\alpha$	$(24a_1)^\alpha$
										$(15b_1)^\beta$	
										$(15b_1)^\alpha$	

[a, b] See Table 3S for the labels.

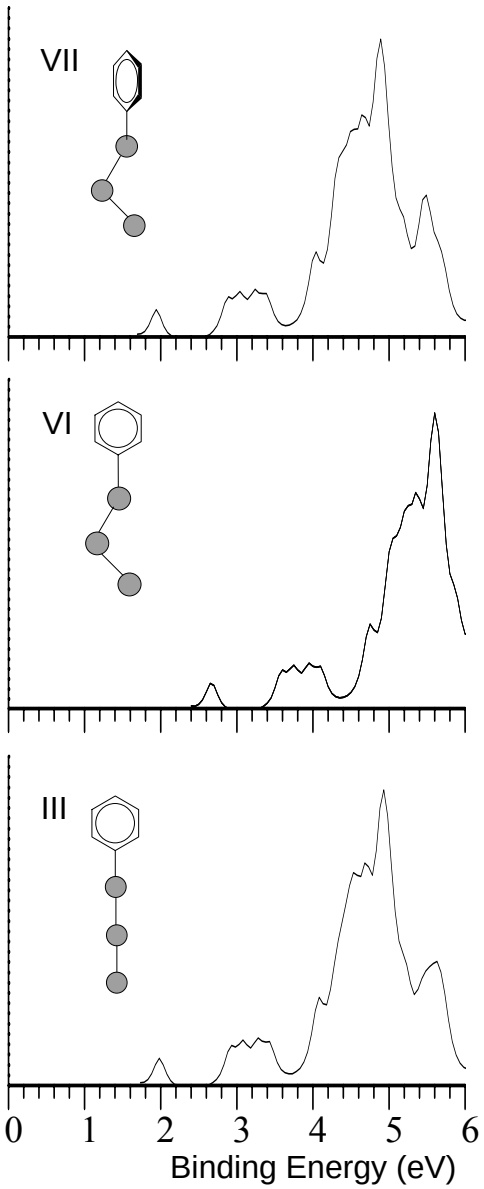

Figure 3S**.** Theoretical generalized Koopman theorem (GKT) – shifted DOS for $Ag_3C_6H_5^-$ (structure III, VI and VII) .

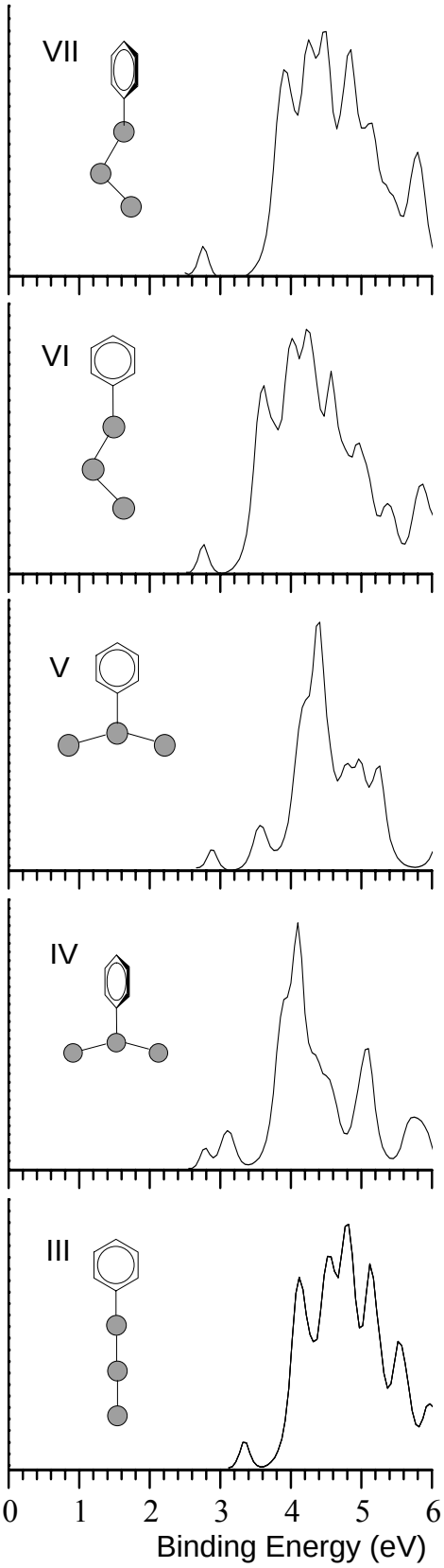

Figure 4S**.** Theoretical generalized Koopman theorem (GKT) – shifted DOS for $Au_3C_6H_5^-$ (structure III-VII).

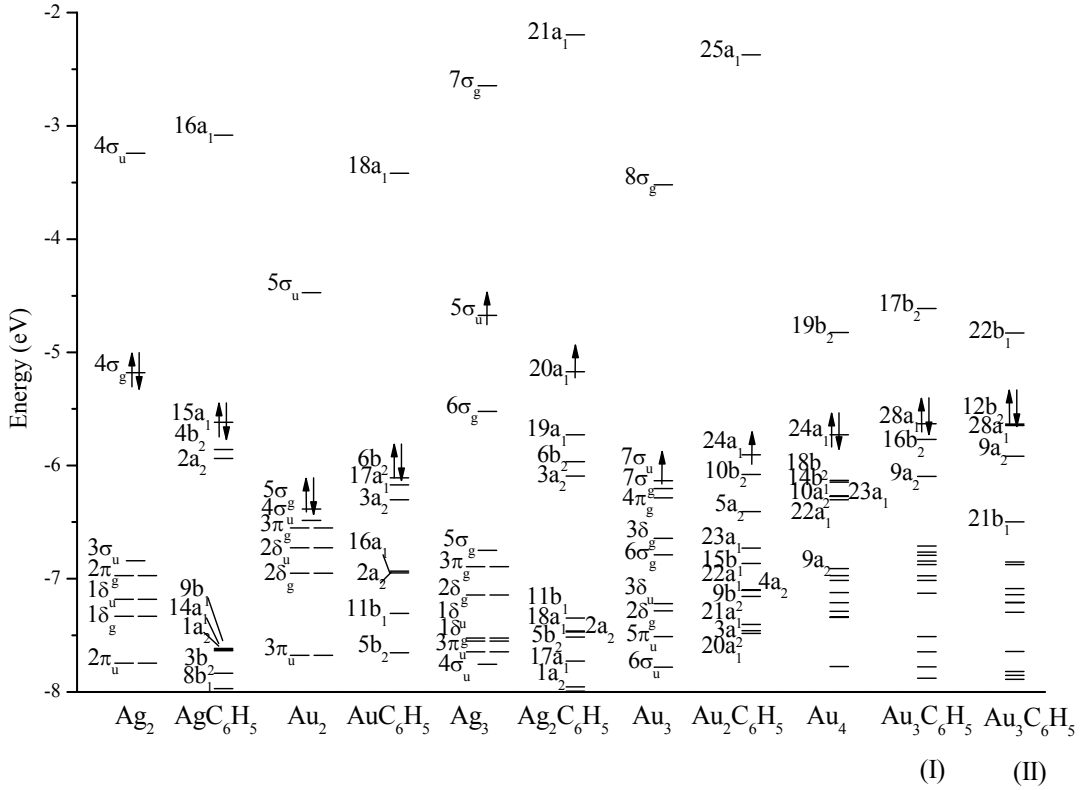

Figure 5S. Energy level diagrams for neutral species calculated at their respectively lowest-lying anionic structure. Occupancy is indicated for the HOMO only, and all lower lying levels are doubly occupied.